Electronic Supplementary information for
Phase transitions on non-uniform curved surfaces:
Coupling between phase and location

Jack O. Law,[1] Jacob M. Dean,[2, *] Mark A. Miller,[2, †] and Halim Kusumaatmaja[1, ‡]

[1]*Department of Physics, Durham University,*
South Road, Durham DH1 3LE, United Kingdom
[2]*Department of Chemistry, Durham University,*
South Road, Durham DH1 3LE, United Kingdom
(Dated: August 6, 2020)

S1.   GLOBAL POTENTIAL ENERGY MINIMA ON THE TORUS

A.   Structure Sequences

We have performed basin-hopping parallel tempering (BHPT) runs as described in the main text to see how the energetically favoured structures evolve with the cluster size. The surface is the 5-7 torus, as used for the case study in the main article, and we compare long- and short-ranged Morse potentials ($\rho = 4$ and $\rho = 18$, respectively) over the range $100 \leq N \leq 500$ particles, which includes the value of $N = 300$, the structures for which are shown in Fig. 7 of the main article. For simplicity, the untruncated potential is used in these optimisations. We depict the optimised structures by their Voronoi tessellations in order to highlight any packing defects without the need to choose a cut-off distance for neighbours. Ill-defined Voronoi cells at the boundary of the clusters have been suppressed, as explained in the main text. This has the effect of removing some cells belonging to edge particles but does not alter the depiction of the cluster interiors.

Fig. S1 shows the lowest-energy structures found for the long-ranged potential. The clusters always adopt compact configurations that reduce their perimeter. Such arrangements require some distortion of the hexagonal packing, but this does not come with an excessive energetic penalty because of the softness of the potential. Small clusters ($N = 100$) form at the "top" or "bottom" of the torus, in the vicinity of zero Gaussian curvature, where they can be both compact and relatively flat. Larger clusters are located on the "outside" of the torus (region of positive Gaussian curvature) in order to remain compact. For sufficiently large clusters, small groups of topological defects arise to accommodate the Gaussian curvature. Each particle in a defect has coordination number $c \neq 6$, giving rise to a topological charge $q = 6 - c$. In Fig. S1, each group of defects has a net charge of $+1$. We find that the number of defects increases with the amount of curvature enclosed: one net fivefold defect (pentagon) at at $N = 300$, two at $N = 400$ and three at $N = 500$. We note that these defects are present for purely energetic reasons; a cluster that does not cover the surface is free to

----

*Current address: Department of Chemistry, University of Bath, Claverton Down, Bath BA2 7AY, United Kingdom

†Electronic address: `m.a.miller@durham.ac.uk`

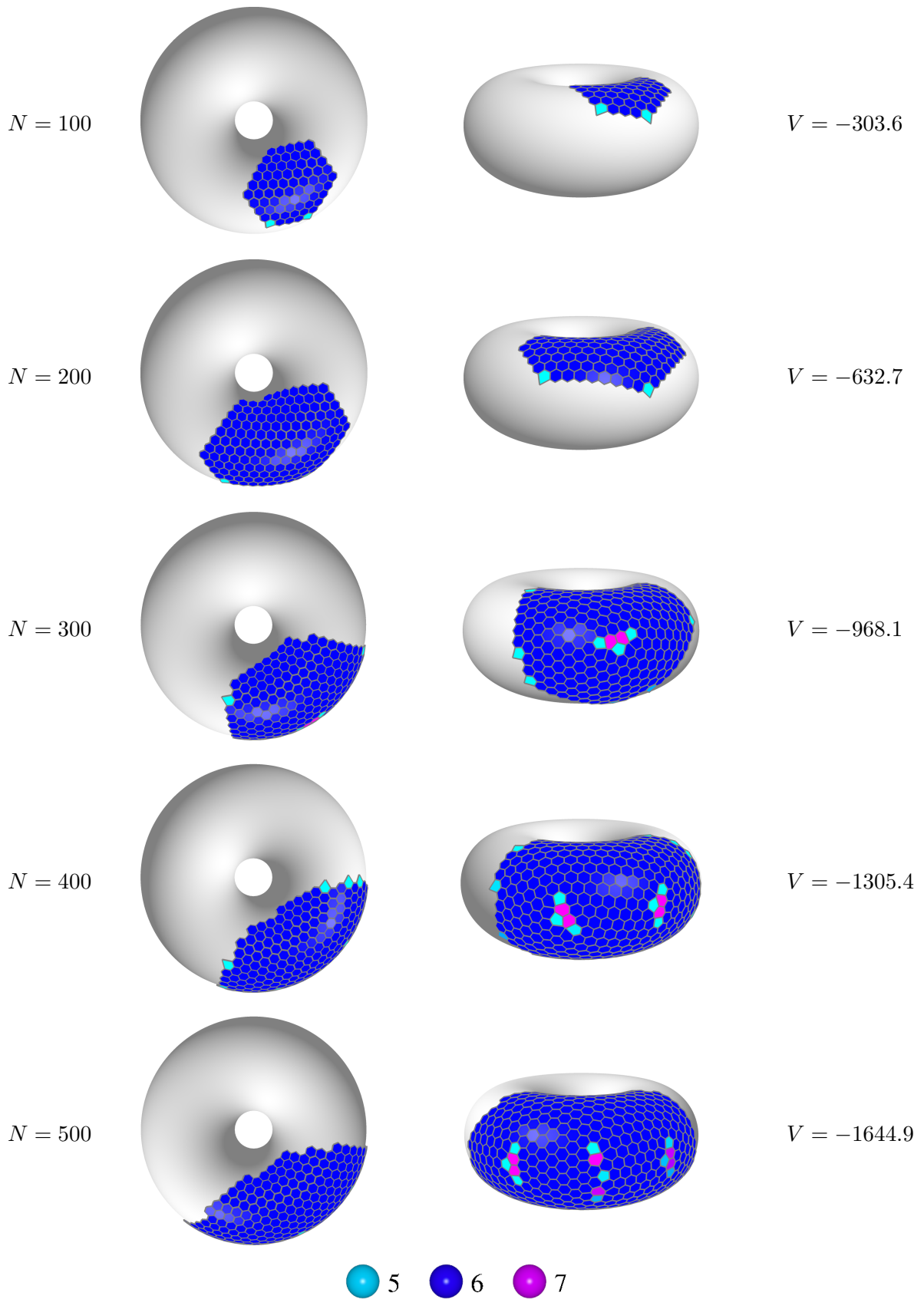‡Electronic address: `halim.kusumaatmaja@durham.ac.uk`

FIG. S1: Putative global potential energy minima for $\rho = 4$ (long-ranged Morse potential), depicted by their Voronoi tessellations. Each row shows the structure for a given number of particles from two perspectives. Cells are coloured by coordination number. The potential energy V is given in units of ε and rounded to one decimal place.

expel defects on any curved surface [1]. Furthermore, a torus has an Euler characteristic of zero so, unlike on a sphere, there is no topological requirement for defects even if the surface is fully covered.

Fig. S2 shows the equivalent sequence of lowest-energy structures for the short-ranged potential. Here, the energetic penalty for distortion of pairwise separations away from the optimal value of r_0 is high. Hence, these clusters avoid topological defects by preferentially occupying the relatively flat region of the torus. The sequence of increasing size N involves elongation of the cluster at the expense of generating a large perimeter. The approximate lattice vectors of the crystal gradually rotate as one follows the cluster round the torus. The incommensurability of the crystal growth leads to a mismatch at the point where the two ends touch at around N= 500, forming a linear defect known as a line slip [2].

There are numerous minor variations on the structures presented in Figs. S1 and S2, often differing in the detail of the perimeter. However, independently seeded BHPT runs do converge to similar energies (differences on the order of ε). Importantly, the overarching features of the structures coming from these repeat runs, such as the location and overall shape of the clusters, are reliably reproducible.

B. Decomposition of the Energy

In the main text we have shown that, at low temperature, increasing the range of the potential ρ leads to a transition between two crystal-like states, C+ and X0 in the case of $N = 300$ particles on the 5-7 torus. We argue that this transition is driven by competition between line energy (the perimeter effect) and crystal frustration (the stress effect). Fig. 7(C) of the main article shows the cross-over in the balance between these effects for the ground-state (zero-temperature) structures as a function of ρ. In this section, we examine the origins of the observed trends in more detail by decomposing the potential energy of the ground states into contributions with a direct physical interpretation.

The energy of each minimum can be broken down into the components

$$E = -3N\varepsilon + E_{\text{line}} + E_{\text{defect}} + E_{\text{stress}} + E_{\text{non-nn}}, \tag{1}$$

which we now describe in turn. In a perfect hexagonal crystal, the interaction energy of any given particle with its immediate neighbours would be -6ϵ. The first term on the right-hand side of Eq. 1 gives this ideal energy for N particles after correcting for double-counting of pairs.

The line tension energy term in Eq. 1 is given by

$$E_{\text{line}} = \frac{\varepsilon}{2} \sum_{\text{edge}} (6 - N_{\text{nn}}), \tag{2}$$

where the sum is over particles on the edge of the cluster. N_{nn} is the number of nearest neighbours (nn) of each particle in the sum (*i.e.*, the number of particles lying closer than $1.45r_0$) and the factor of $1/2$ corrects for double-counting of bonds. We identify particles on the edge using a test-particle method. For each pair of nearest neighbours, a test particle is inserted on the surface at the two locations where it is at a distance r_0 from both real particles in the pair. If the test particle overlaps with another real particle in exactly one of these locations then both particles in the pair are designated as lying on the edge of the cluster.

$N = 100$ $V = -262.8$

$N = 200$ $V = -538.3$

$N = 300$ $V = -812.9$

$N = 400$ $V = -1087.8$

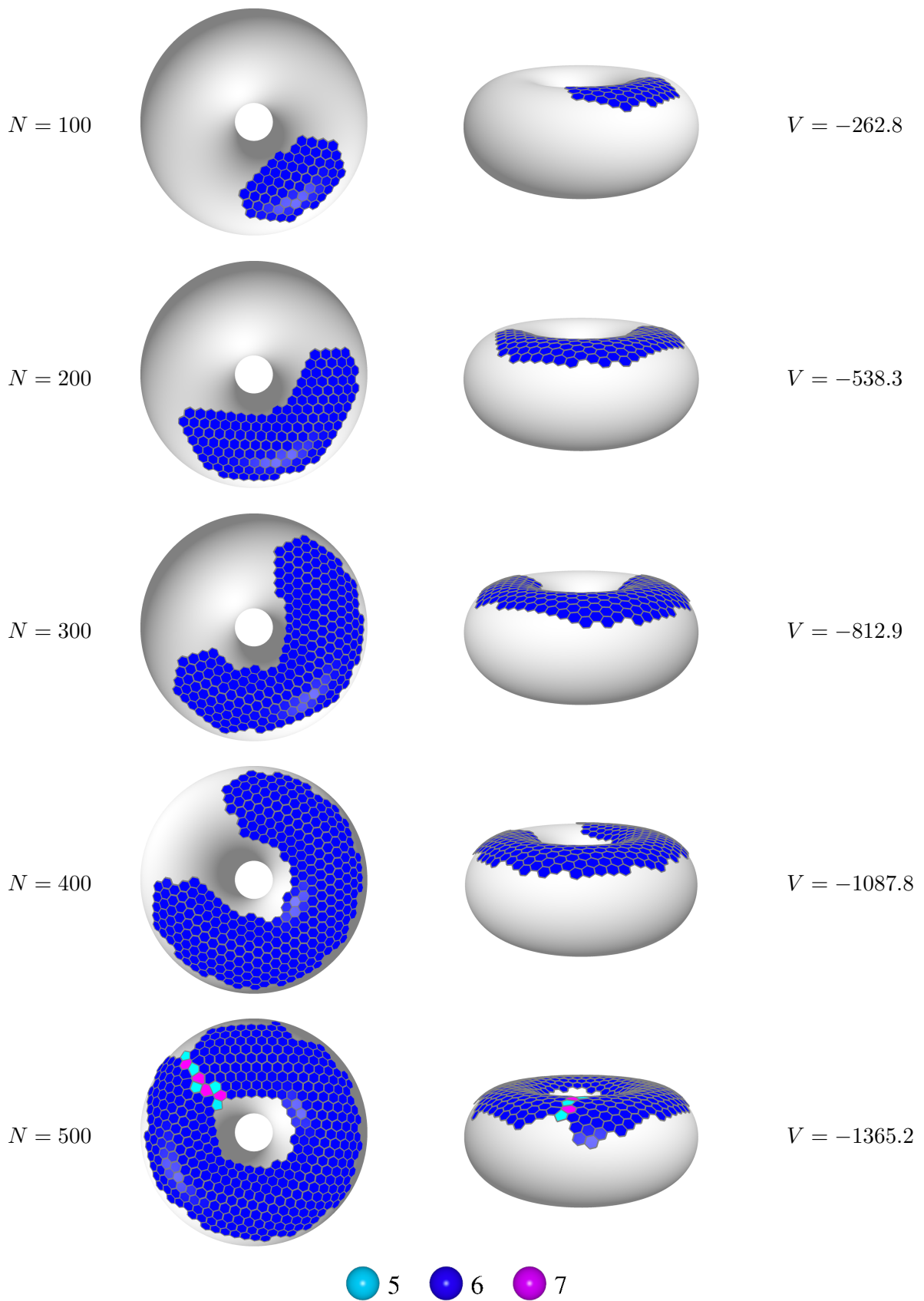$N = 500$ $V = -1365.2$

5   6   7

FIG. S2: Putative global potential energy minima for $\rho = 18$ (short-ranged Morse potential), depicted by their Voronoi tessellations. Each row shows the structure for a given number of particles from two perspectives. Cells are coloured by coordination number. The potential energy V is given in units of ε and rounded to one decimal place.
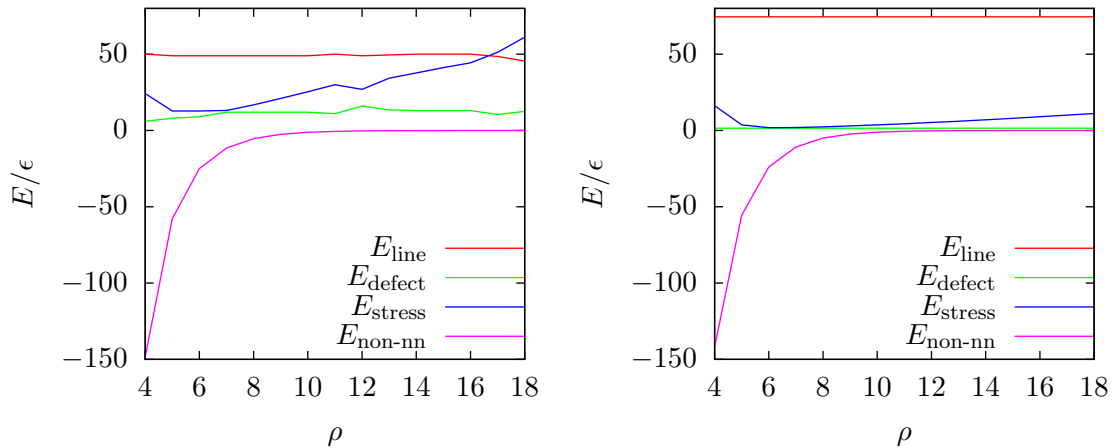
FIG. S3: Left: Components of the potential energy for the C+ state for $N = 300$ particles on the 5-7 torus as a function of the potential range parameter ρ. Right: Components of the potential energy for the X0 state.
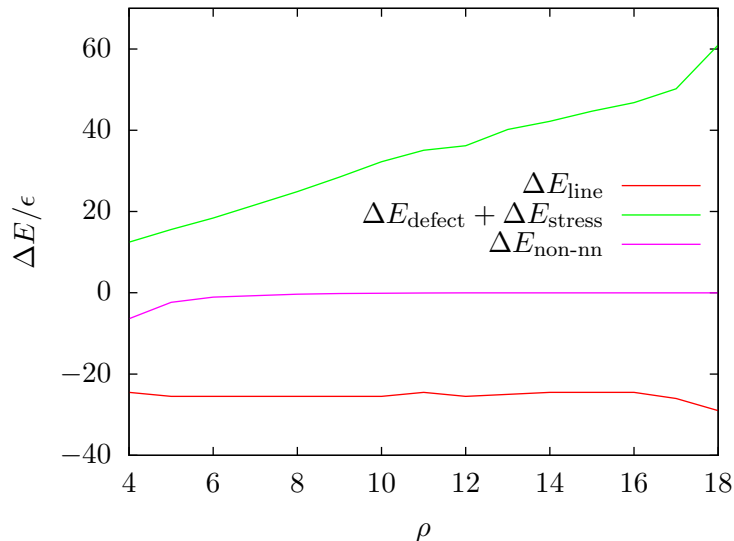

FIG. S4: The change in potential energy, $\Delta E = E_{C+} - E_{X0}$, from the X0 to the C+ state for the perimeter effect (line energy), stress effect (including defects), and the non-nearest-neighbour interactions ($\Delta E_{\text{non-nn}}$).

The defect energy term in Eq. 1 corresponds to energy contribution from particles that have a number of nearest neighbours different from 6,

$$E_{\text{defect}} = \frac{\varepsilon}{2} \sum_{\text{not edge}} (6 - N_{\text{nn}}), \tag{3}$$

where the sum is over all particles not on the edge of the cluster.

The stress energy term in Eq. 1 captures the excess energy of nearest-neighbour pairs

whose separation is different from the equilibrium distance,

$$E_{\text{stress}} = \sum_{\text{nn}} (U_{\text{M}} + \epsilon),$$

where the sum is over pairs of nearest neighbours.

Finally, the non-neighbours energy term in Eq. 1,

$$E_{\text{non-nn}} = \sum_{\text{non-nn}} U_{\text{M}},$$

captures the interactions between all pairs of particles that are not nearest neighbours.

This breakdown is presented for the C+ and X0 states as a function of ρ in Fig. S3. In Fig. S4 we also plot the energy difference between C+ and X0 for E_{line} (the perimeter effect), $E_{\text{defect}} + E_{\text{stress}}$ (the stress effect), and $E_{\text{non-nn}}$. In agreement with the discussion in Sec. S1 A, the X0 structures have no defect energy and are only weakly stressed, but at the expense of a more elongated shape with a higher line energy. In contrast, for the C+ state, the line energy is lower, but it has higher E_{defect} and E_{stress}. For both structures, the line energy in these zero-temperature structures does not vary much with ρ because the structures do not undergo significant rearrangement when relaxed at different ρ.

$E_{\text{non-nn}}$ varies with ρ, especially for low ρ where the range of interaction is larger than the typical equilibrium distance between any pair of neighbouring particles. However, $E_{\text{non-nn}}$ has a similar dependence for the X0 and C+ states, leading to a small $\Delta E_{\text{non-nn}}$. Thus, we conclude this term does not play a major role in the transition between the X0 and C+ states.

Overall, the increase in $E_{\text{defect}} + E_{\text{stress}}$ against nearly static differences in E_{line} and $E_{\text{non-nn}}$ drives the transition from C+ to X0 crystal-like structures with increasing ρ.

S2. ORDER PARAMETER DISTRIBUTIONS

Throughout this work we have used the the local bond order parameter $|\psi|$, defined in Sec. 3.1 of the main article, to define whether a given particle is in a crystalline environment. In this section, we examine the full distribution of $|\psi|$ and, in particular, what changes in the distribution can tell us about microstructure as we traverse the major phase transitions on the 5-7 torus.

Fig. S5(A) shows histograms of $|\psi|$ over a range of temperatures that spans the G, L$-$ and C+ states at $\rho = 5$. Each histogram has 7 peaks or steps. From left to right, these features arise from particles with 0 to 6 maximally ordered neighbours. The region to the left of a particular peak is dominated by contributions from particles that have the same number of neighbours, but some deviation from perfect hexagonal ordering. In the gas state (for example, at $k_{\text{B}}T/\varepsilon = 0.56$), there is a sharp peak around $|\psi| = 0.33$, which represents particles with two nearest neighbours in a configuration characteristic of hexagonal order. This indicates that the second most common motif (after isolated particles) is a group of three particles arranged in an equilateral triangle. As the temperature is reduced, the height of this peak deceases rapidly as the particles condense into the liquid phase. The histogram becomes relatively flat, with less pronounced peaks, since particles have a range of coordination numbers and little crystalline order. This change happens smoothly, meaning the transition from G to L$-$ cannot be pinpointed from the bond-order distribution. As the
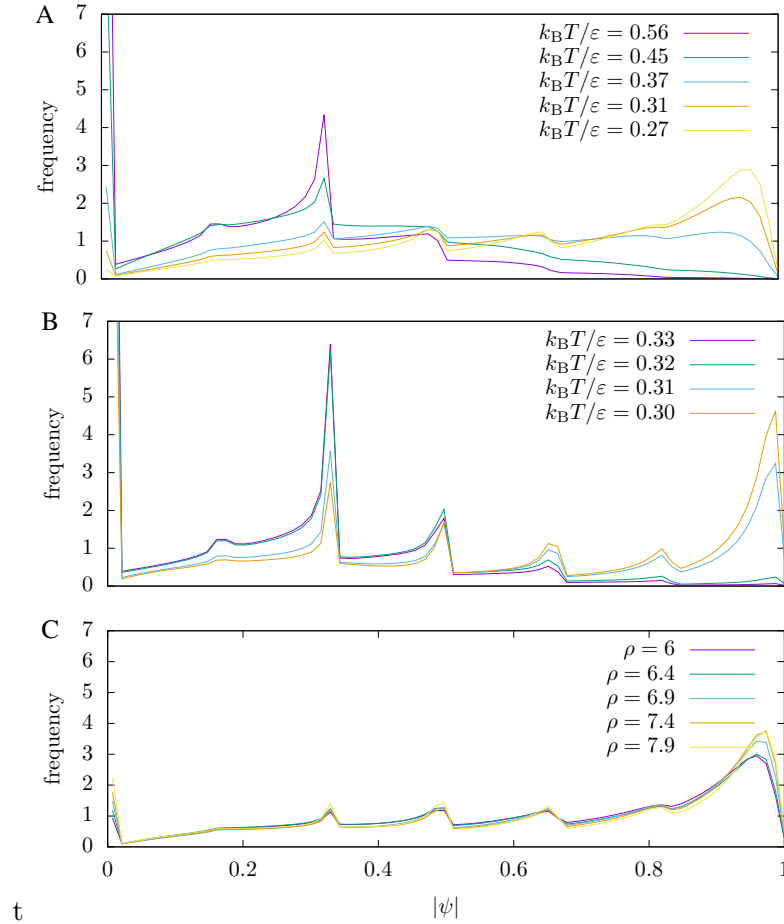
FIG. S5: Normalised histograms of the per-particle bond order parameter $|\psi|$ (defined in Sec. 3.1 of the main article) from simulations of 300 particles on a 5-7 torus in the canonical ensemble. (A) Potential range parameter $\rho = 5$ over a range of temperatures; the crystal peak (just below $|\psi| = 1$), is broad and grows gradually with decreasing temperature. (B) At $\rho = 16$ over a smaller range of temperatures; the crystalline peak emerges rapidly and is sharp. (C) At $k_B T = 0.29$ for different potential ranges; the profiles are similar, although the peaks become slightly sharper with increasing ρ.

temperature drops further, the peak near $|\psi| = 1$ becomes dominant, indicating that the cluster has an increasingly dense, crystalline structure. In addition, all the peaks become sharper, reflecting the presence of particles with crystalline order but missing neighbours, such as particles at the edges of the cluster. As the potential is soft, the peaks are quite broad because the structure still contains some disorder.

Fig. S5(B) shows histograms taken at shorter potential range, $\rho = 16$, over a much narrower range of temperatures around the G to X0 transition. It can be seen that the transition is much sharper than for the softer potential in panel (A). While the profiles of the gas phases in panels (A) and (B) are similar, the crystal phase in (B) features much sharper peaks, indicating strong crystalline order. Most particles have six neighbours, but there are also clear peaks for the boundary particles at three, four and five neighbours. There are also significant peaks at the zero and one neighbour positions, unlike for the crystal phase at $\rho = 5$. This suggests that the crystalline cluster is coexisting with a significant amount

TABLE I: Summary of nomenclature for states of the system. The first symbol represents the thermodynamic phase. The second symbol denotes the sign of the Gaussian curvature in the region where the state is found.

Symbol	Explanation
G	gas (covers whole surface)
L	liquid
C	condensed
X	crystal
+	positive Gaussian curvature
−	negative Gaussian curvature
0	zero Gaussian curvature (and vicinity)
±	both positive and negative Gaussian curvature

of gas at the lowest temperature included on the plot.

Fig. S5(C) shows histograms taken at a cross-section of values of ρ around the transition from C+ to X0. Although the peaks become slightly sharper at higher ρ, the effect is small. This shows that the C+ to X0 transition, which involves a major relocation and rearrangement of the structure, has little effect on the microstructure of the cluster. We have seen that the bond-order distribution reflects the microstructure of the system, but, significantly, cannot be used in isolation to identify the state of the system in full. Hence, a second, positional, order parameter is needed to understand these transitions (see the free energy surfaces in Fig. 4 of the main article).

S3.   ADDITIONAL PHASE PHASE DIAGRAMS

In this section we present some additional phase diagrams to show how the coupling of phase and location is affected by the number of particles and the precise shape of the surface. As in the main paper, states are labelled with two symbols to denote the phase of matter and the location. For convenience, a summary of these symbols is repeated in Table I.

A.   Planar surface

As a reference system without the effects of curvature, we present the phase diagram of 300 Morse particles on a planar surface in Fig. S6. The simulation cell has periodic boundary conditions in both directions and an edge length of $37.17 r_0$, giving it an area equal to that of the main test case of the 5-7 torus. The similarities and differences between the planar and toroidal cases are covered in the main article.

B.   5-7 Torus with 100 Particles

The phase diagram for a 5-7 torus with 100 Morse particles (fewer than in the main article) is shown in Fig. S7, with snapshots of the three observed states shown in Fig. S8. Although free energy calculations show that the L− state continues to exist as a metastable
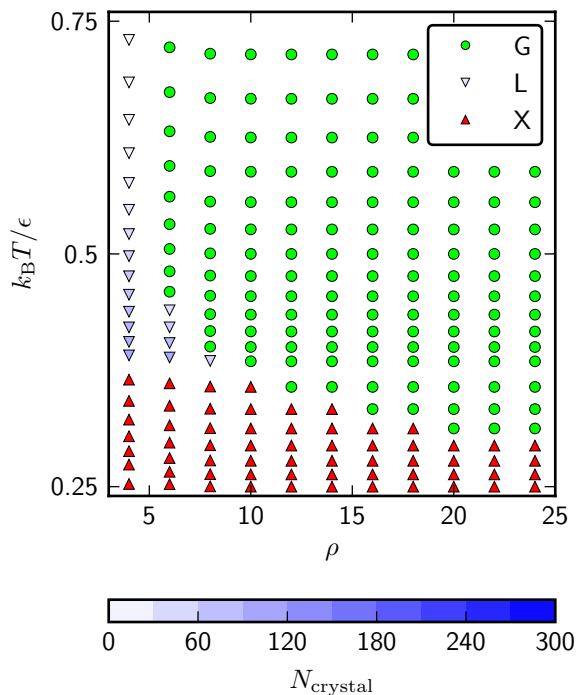
FIG. S6: Phase diagram for 300 Morse particles on a plane with periodic boundaries and an area equal to that of a 5-7 torus as a function of the potential range parameter ρ and the reduced temperature $k_{\mathrm{B}}T/\varepsilon$.

state, it has a higher free energy than the C+ state, and hence it does not appear in the phase diagram.

We further find that, with decreasing temperature, the X0 state extends to lower values of ρ than in the case of 300 particles. This observation is consistent with the ground-state (*i.e.*, zero temperature limit) structures shown in Fig. S1; at $\rho = 4$ the lowest-energy structure for $N = 100$ crystal is located in the vicinity of zero Gaussian curvature, whereas for $N = 300$ it has moved to the region of positive Gaussian curvature. Moreover, unlike the case of 300 particles, the boundary between the C+ and X0 phases for $N = 100$ is not independent of temperature. To explain these observations, consider a C+ state on the outside of the torus for a relatively low ρ. Decreasing the temperature drives the system towards increasing crystallinity. For a small number of particles, such as $N = 100$, this can be achieved by migrating to the "top" or "bottom" of the torus for two reasons: first, the crystal in the X0 state is less stressed due to Gaussian curvature. Secondly, the difference in perimeter, and hence line energy, between the C+ and X0 states is small. Thus, the strain effect can dominate over the perimeter effect. In contrast, for a larger number of particles (such as for $N = 300$), the line energy penalty becomes prohibitively expensive in the X0 state, since the shape of the cluster is highly anisotropic with a large aspect ratio. Therefore, for $N = 300$, the system instead creates defects to compensate for the increasing degree of crystallinity in the C+ state with decreasing temperature.

The transition from C+ to X0 can be induced by increasing ρ, since the elastic energy for stressing the crystal and/or creating defects becomes more expensive than the line energy
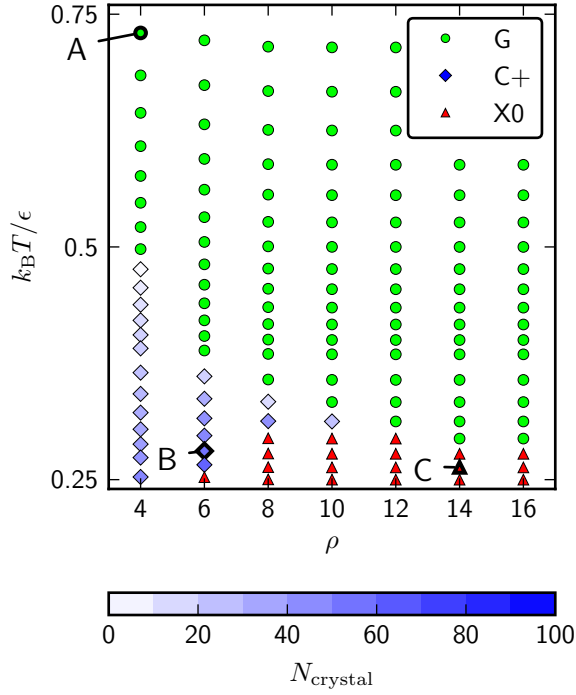
FIG. S7: Phase diagram for 100 Morse particles on a 5-7 torus as a function of the potential range parameter ρ and the reduced temperature k_BT/ε. Snapshots of the system at the labelled points are shown in Fig. S8.
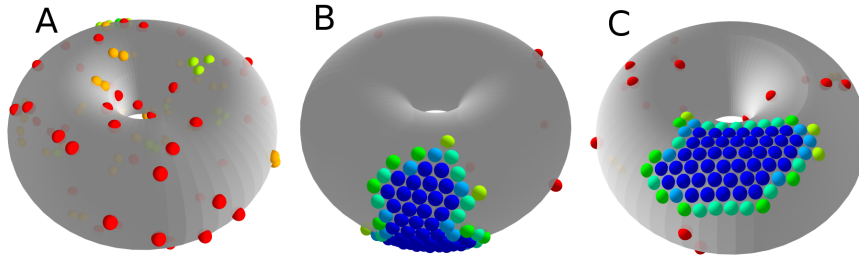

FIG. S8: Snapshots of the states labelled in the phase diagram of Fig. S7 for 100 Morse particles on the 5-7 torus. (A) G, at $\rho = 4$, $k_BT/\varepsilon = 0.73$; (B) C+, at $\rho = 6$, $k_BT/\varepsilon = 0.28$; (C) X0, at $\rho = 14$, $k_BT/\varepsilon = 0.26$. Particles are coloured by the number of nearest neighbours.

penalty when the potential is short-ranged. The C+ to X0 phase boundary will tend to become more independent of temperature for larger crystals.

C. 5-7 Torus with 500 Particles

As an example of a larger cluster, we have also investigated the case of 500 Morse particles on the 5-7 torus. Once again, the key message is that we observe a localisation of the particles
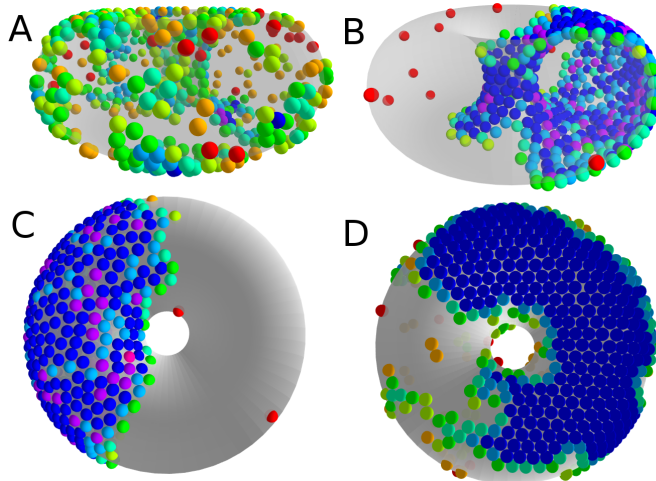
FIG. S9: Snapshots of the states labelled in the phase diagram of Fig. S10 for $N = 500$ particles on the 5-7 torus. (A) G, at $\rho = 4$, $k_{\mathrm{B}}T/\varepsilon = 0.73$; (B) L±, at $\rho = 4$, $k_{\mathrm{B}}T/\varepsilon = 0.44$; (C) C+, at $\rho = 4$, $k_{\mathrm{B}}T/\varepsilon = 0.36$; and (D) X0, at $\rho = 14$, $k_{\mathrm{B}}T/\varepsilon = 0.33$. Particles are coloured by the number of nearest neighbours.

caused by the curvature of the surface, but the specific details are affected by the additional particles. In Fig. S9 we show snapshots of the four observed states. Free energy calculations confirm that these phases are separated by barriers and are therefore distinct. At high temperature, we observe a gas (now rather dense) as usual. For the liquid phase, instead of just occupying the region of negative Gaussian curvature (L− phase), the additional particles lead to a second loop that wraps around the tube of the torus, forming what we term the L± state to signify the fact that it covers regions both of negative and of positive Gaussian curvature. The closure of this second loop reduces the total perimeter of the cluster in comparison to an L− phase that extends too far from the centre of the torus. The C+ and X0 phases appear similarly to the 300 particle case. The transition between these two states is also independent of temperature for $N = 500$, for the reasons given in the previous subsection. The phase diagram for a 5-7 torus with 500 particles is shown in Fig. S10.

D. The 3.5-10 Torus with 300 Particles

We have shown that surface curvature leads the localisation of thermodynamic states. By comparing the case of the 5-7 torus and the sinusoidal surface in the main text, it can be seen that the number and character of those states depends on the nature of the surface. Even for toroidal surfaces, different conditions can be produced by altering the size and aspect ratio of the torus. In this section, we investigate the 3.5-10 torus (radii $a = 3.5r_0$ and $c = 10r_0$ as defined in Fig. 1 of the main text) for $N = 300$ particles and show that its phase diagram has some different features from that of the 5-7 torus.

The 3.5-10 torus has the same surface area as the 5-7 torus, but consists of a longer, thinner tube. We observe three states, shown as snapshots in Fig. S11. These are a gas (G), a condensed state wrapped around tube of the torus (C±), and an X0 state. Fig. S12 shows the phase diagram. The loss of the L− and C+ state in favour of the wrapped state can easily be understood in terms of line energy. As the bore of the torus is so wide, an

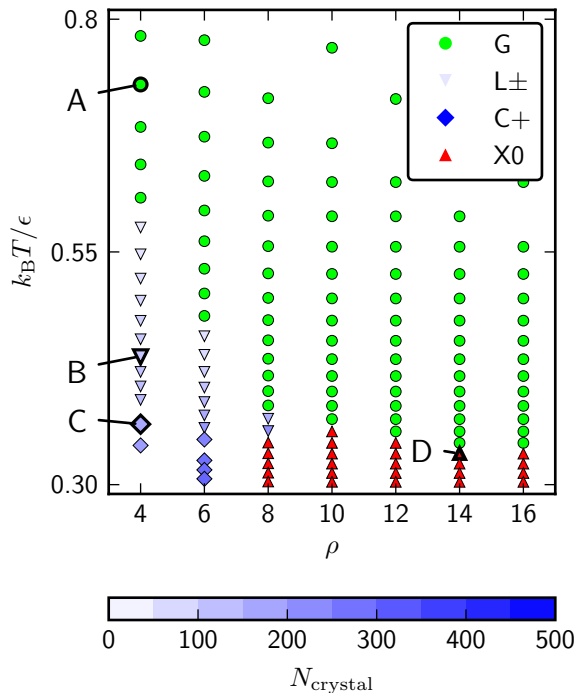FIG. S10: Phase diagram for 500 Morse particles on a 5-7 torus as a function of the potential range parameter ρ and the reduced temperature k_BT/ε. Snapshots at the points labeled A–D are given in Fig. S9.

L− state would have a large perimeter; and as the tube is so thin, a C+ state would have a very large aspect ratio. However, the thinness of the tube stabilizes the C± state as its perimeter is relatively small. The frustration of the crystal is also lower, as the Gaussian curvature of this torus is relatively low. Hence, the X0 state only becomes the stable phase at higher ρ, compared to a 5-7 torus.
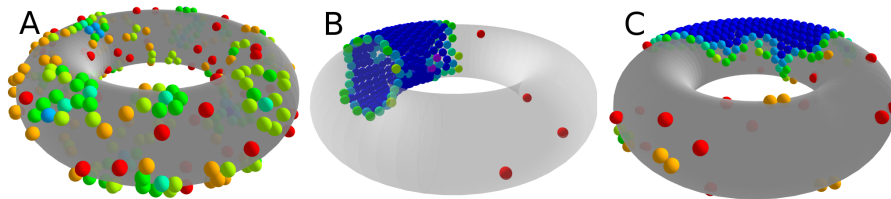

FIG. S11: Snapshots of the states labelled in the phase diagram of the 3.5-10 torus with $N = 300$ in Fig. S12. (A) G, at $\rho = 4$, $k_BT/\varepsilon = 0.78$; (B) C±, at $\rho = 6$, $k_BT/\varepsilon = 0.30$; and (C) X0, at $\rho = 12$, $k_BT/\varepsilon = 0.30$. Particles are coloured by the number of nearest neighbours.
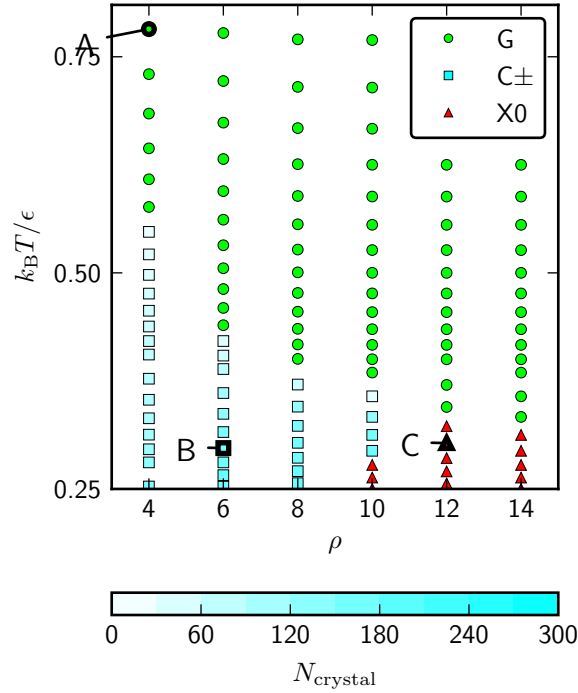
FIG. S12: Phase diagram for $N = 300$ Morse particles on a 3.5-10 torus as a function of the potential range parameter ρ and the reduced temperature k_BT/ε. Snapshots from the points labelled A–C are shown in Fig. S11

S4. VIDEOS OF PHASE TRANSITIONS ON THE TORUS

The movie files in the electronic supplementary information illustrate the following transitions on the 5-7 torus as observed in equilibrium molecular dynamics simulations. In all cases, particles are coloured by coordination number using the scale given in Fig. 2 of the main article.

1. Transition from the C+ state to the L− state at $\rho = 6$ and $k_BT/\varepsilon = 0.38$.

2. Transition from the C+ to the X0 state at $\rho = 7$ and $k_BT/\varepsilon = 0.25$.

3. Transition from the G to the X0 state at $\rho = 20$ and $k_BT/\varepsilon = 0.3$.

[1] S. Li, R. Zandi, A. Travesset, and G. M. Grason, Phys. Rev. Lett. **123**, 145501 (2019).
[2] D. A. Wood, C. D. Santangelo, and A. D. Dinsmore, Soft Matter **9**, 10016 (2013).